Release of long-range tertiary interactions potentiates aggregation of natively unstructured α-synuclein

Carlos W. Bertoncini*†, Young-Sang Jung†, Claudio O. Fernandez‡, Wolfgang Hoyer*, Christian Griesinger†, Thomas M. Jovin*, and Markus Zweckstetter†§

Departments of *Molecular Biology and †NMR–Based Structural Biology, Max Planck Institute for Biophysical Chemistry, Am Fassberg 11, D-37077 Göttingen, Germany; and ‡Instituto de Biología Molecular y Celular de Rosario, Universidad Nacional de Rosario, Suipacha 531, S2002LRK Rosario, Argentina

Edited by Gregory A. Petsko, Brandeis University, Waltham, MA, and approved December 21, 2004 (received for review September 27, 2004)

In idiopathic Parkinson's disease, intracytoplasmic neuronal inclusions (Lewy bodies) containing aggregates of the protein α-synuclein (αS) are deposited in the pigmented nuclei of the brainstem. The mechanisms underlying the structural transition of innocuous, presumably natively unfolded, αS to neurotoxic forms are largely unknown. Using paramagnetic relaxation enhancement and NMR dipolar couplings, we show that monomeric αS assumes conformations that are stabilized by long-range interactions and act to inhibit oligomerization and aggregation. The autoinhibitory conformations fluctuate in the range of nanoseconds to microseconds corresponding to the time scale of secondary structure formation during folding. Polyamine binding and/or temperature increase, conditions that induce aggregation *in vitro*, release this inherent tertiary structure, leading to a completely unfolded conformation that associates readily. Stabilization of the native, autoinhibitory structure of αS constitutes a potential strategy for reducing or inhibiting oligomerization and aggregation in Parkinson's disease.

amyloid | fibrillation | Parkinson's disease

Parkinson's disease (PD) is the second most common neurodegenerative disease and the most common movement disorder, affecting 1–2% of the population over 65 years of age (1). The cause of PD is as yet unclear due in part to a complex etiology involving a combination of genetic susceptibility and numerous environmental factors (2). Proteinaceous aggregates in motor neurons of the substantia nigra and locus coeruleus are characteristic of idiopathic PD. An abundant component of these so-called Lewy bodies is the presynaptic protein α-synuclein (αS) (3). Three genetic mutations in αS (A30P, E46K and A53T) have been identified in autosomal-dominantly inherited early-onset PD (4, 5). *In vitro*, different conditions such as increased temperature, lower pH, and naturally occurring polyamines accelerate αS aggregation (6, 7). Compelling evidence now supports a cytotoxic role in PD for protofibrils, early oligomers of αS (8).

In other amyloid-related neurological disorders, such as Creutzfeldt–Jakob disease, protein oligomerization/aggregation requires destabilization of a soluble monomeric protein followed by the formation of highly ordered, β-sheet-like fibrillar structures (9). αS, however, belongs to the class of natively unfolded proteins with no apparent ordered secondary structure detectable by far-UV CD, Fourier transform IR, or NMR spectroscopy (6, 10, 11), although recent evidence indicates the existence of distinct, functionally relevant intramolecular interactions (refs. 7 and 12 and this work). The challenge is to rationalize in structural terms the inactive state of the soluble, unstructured protein and the potentiation of aggregation by point mutations, ligand binding, or changes in solution conditions.

During the past decade numerous NMR techniques have been developed for elucidating the unfolded states of proteins in atomic detail (13). ^{15}N-relaxation time measurements and paramagnetic relaxation enhancement (PRE) from site-directed spin labeling allowed the detection of native-like contacts and hydrophobic clusters in denatured proteins (14, 15). In addition, measurement of residual dipolar couplings (RDCs) in a weakly aligned protein provides long-range orientational information and may reveal residual native-like topology in the unfolded states of proteins (16, 17).

Here, we use PRE from site-directed spin labeling and RDCs to characterize the ensemble of conformations that αS assumes in its natively unfolded state as well as the early transitions that lead to oligomerization and aggregation.

Experimental Procedures

Protein Preparation. The coding sequence for WT human αS in the plasmid pT7–7 was kindly provided by the Lansbury Laboratory, Harvard Medical School, Cambridge, MA. Three different αS cysteine-containing mutants (A18C, A90C, and A140C) were constructed by using the QuikChange site-directed mutagenesis kit (Stratagene), and the introduced modifications were verified by DNA sequencing. ^{15}N- and ^{13}C/^{15}N-labeled αS, WT and mutants, were expressed in *Escherichia coli* grown in M9 minimal medium supplemented with $^{15}NH_4Cl$ or $^{15}NH_4Cl$ and ^{13}C-D-glucose (Cambridge Isotope Laboratories, Cambridge, MA) and purified as described (18). The C-terminal αS peptide comprising residues 105–136 was synthesized by K. Overkamp (Max Planck Institute for Biophysical Chemistry) by using standard solid-phase fluorenylmethoxycarbonyl chemistry. The peptide was purified by semipreparative reverse-phase HPLC, and the purity (>95%) was analyzed by MS. Natural polyamines were obtained from Sigma.

Spin Labeling of αS. The reaction of the αS cysteine-containing mutants with the nitroxide spin label MTSL (1-oxy-2,2,5,5-tetramethyl-D-pyrroline-3-methyl)-methanethiosulfonate (Toronto Research Chemicals, Toronto) was carried out essentially as described (19) with some modifications. Briefly, DTT was removed before labeling from the buffer by using size exclusion chromatography (PD-10 columns, Amersham Pharmacia Biosciences), and the proteins were equilibrated in 20 mM Tris·HCl buffer, pH 7.5, and 100 mM NaCl. Free sulfhydryl groups were reacted with a 5-fold molar excess of the MTSL solubilized in acetone, at 4°C for 16 h. Unreacted spin label was removed by using PD-10 columns, and spin-labeled proteins were concentrated by using Microcon YM-3 (molecular weight cutoff, 3,000)

This paper was submitted directly (Track II) to the PNAS office.

Abbreviations: αS, α-synuclein; PD, Parkinson's disease; RDC, residual dipolar coupling; PRE, paramagnetic relaxation enhancement; MTSL, 1-oxy-2,2,5,5-tetramethyl-D-pyrroline-3-methyl)-methanethiosulfonate; HSQC, heteronuclear single quantum coherence; NAC, non-Aβ component of Alzheimer's disease amyloid.

§To whom correspondence should be addressed. E-mail: mzwecks@gwdg.de.

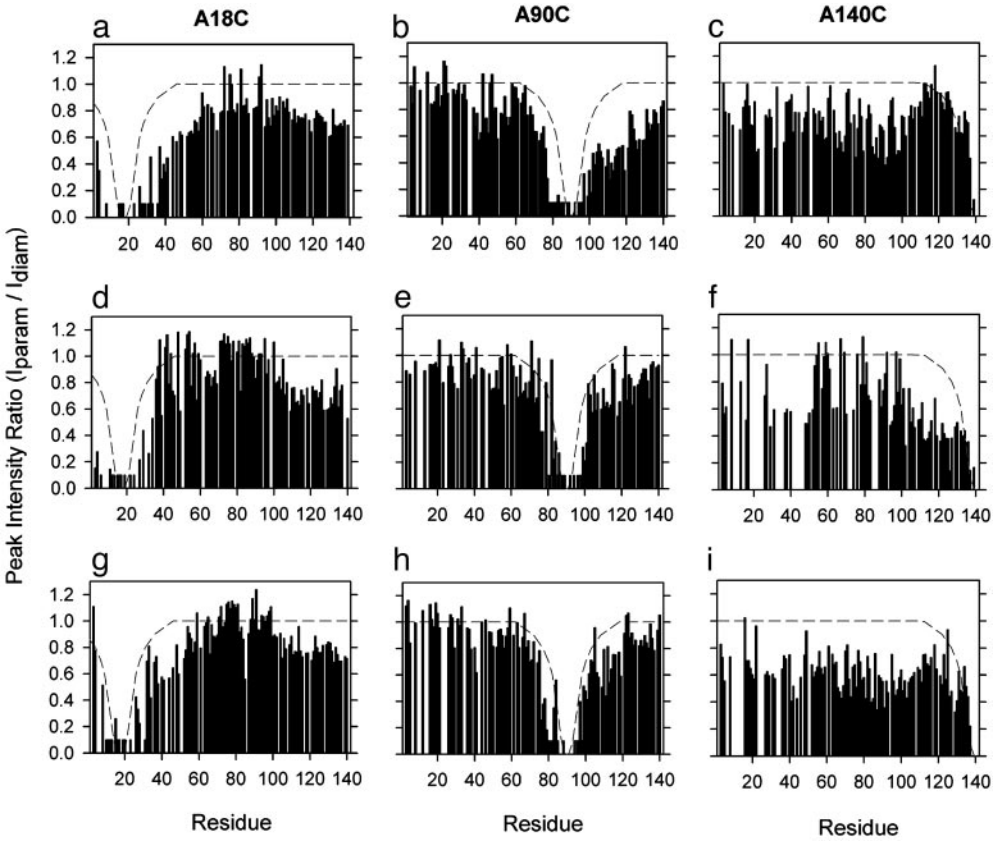

Fig. 1. PRE of amide protons in spin-labeled αS. Three cysteine mutants of αS (A18C, A90C, and A140C) were labeled with MTSL. HSQC spectra in the presence (paramagnetic) and absence (diamagnetic) of spin label were recorded at 15°C, and the intensity ratio (I_{param}/I_{diam}) of the resonance peaks was determined. Dashed lines indicate paramagnetic effects expected for a random coil polypeptide (34). (*a–c*) αS in buffer A. (*d–f*) αS in buffer A plus 8 M urea. (*g–i*) αS in buffer A plus 6 mM spermine.

(Amicon). In addition, a second nitroxide spin label, PROXYL (Aldrich), was used by following the same labeling procedures. Complete labeling with the nitroxide radical was verified by MS.

Diamagnetic states were measured by using unlabeled cysteine-mutant proteins in the presence of 0.5 mM DTT.

Alignment of αS in Anisotropic Media. RDCs were measured in αS aligned in 10 mg/ml of bacteriophage Pf1 (Asla, Riga, Latvia) (20) and in 5% (wt/vol) *n*-octyl-penta(ethylene glycol)/octanol (C8E5) (Sigma) (21). Alignment in the presence of urea was performed by the addition of octanol to the sample-urea-penta-ethylene glycol solution. Changing the alignment medium to 5% (wt/vol) *n*-dodecyl-penta(ethylene glycol)/hexanol (Sigma) (21) allowed RDC measurements at higher temperatures.

NMR Measurements. NMR spectra were acquired at 15°C on Bruker Avance 600 and 700 NMR spectrometers. Aggregation did not occur under these conditions of low temperature and absence of stirring. All NMR experiments were performed on a 100-μM sample of αS in buffer A (25 mM Tris·Cl, pH 7.4/0.1 M NaCl).

PRE effects were measured from the peak intensity ratios between two 2D ^{15}N-^{1}H heteronuclear single quantum coherence (HSQC) NMR spectra acquired in the presence and absence of the nitroxide radical. The intensity ratios shown in Fig. 1 are averages over repeated measurements for up to three different protein preparations.

One-bond N–H RDCs (D_{NH}) were determined by using the IPAP ^{15}N-HSQC sequence (22). A 3D HNCACB experiment was used to facilitate backbone assignments under denaturating conditions (23). All spectra were processed and analyzed by using NMRPIPE (24) and NMRVIEW (25). D_{NH} values were calculated as the difference between splittings measured in an aligned sample and those measured in an isotropic sample (i.e., the RDCs were not corrected for the negative gyromagnetic ratio of ^{15}N). RDCs observed under different conditions were normalized based on the size of the splitting of the deuterium signal (relative to RDCs for free αS in buffer A).

Calculation of Distance Restraints. Distance restraints were calculated as described from the intensity ratio between two ^{15}N-^{1}H HSQC NMR spectra, in the diamagnetic and paramagnetic states of the protein (26). For amides that were broadened beyond detection in the oxidized spectra, an upper limit for the intensity ratio was estimated from the spectral noise in the oxidized spectrum. Experimental values for the intrinsic transverse relaxation rates (11) were used for conversion of intensity ratios into PREs. The correlation time for the electron-nuclear interaction τ_c was set to 4 ns, in agreement with previous studies (26).

Structure Determination and Analysis. Structure calculations were performed by using XPLOR-NIH, version 2.0.6 (27). Torsion angle dynamics were started at 3,000 K from a random coil conformation with the temperature reduced to 20 K during simulated annealing, followed by a short energy minimization. An all-atom representation of αS was used. Structural energy terms from steric repulsion, bond length, bond angles, dihedral angles, and favored regions of the Ramachandran map were used.

Intensity ratios for almost the whole N terminus of A140C αS

were <0.8 (Fig. 1*c*). To avoid an overly restrained structure, only intensity ratios <0.75 were regarded as significant for this mutant, whereas a cutoff of 0.8 was allowed for the A18C and A90C mutants. However, changing these cutoff values in a reasonable range did not change the main structural features. Peaks with intensity ratios below these cutoffs were restrained to the calculated distance ±5 Å by using a harmonic square well potential. For intensity ratios above these cutoffs, a target distance was calculated from an intensity ratio of 0.9, and the lower distance bound was restrained to −5 Å of the calculated value. All distances were imposed as restraints between the backbone amide proton of the residue with the cysteine-MTSL group and residue-specific amide protons.

Structure calculations were also performed with a modified version of the *ab initio* structure prediction program ROSETTA that allows inclusion of experimental distance restraints (28, 29). In using ROSETTA we assumed that despite the high conformational flexibility present in αS all residues favor a distribution of dihedral angles corresponding to those seen in structures of native proteins in agreement with previous studies (30). Distance restraints were imposed as described above with the modification that no lower bounds were enforced.

Clustering was performed by using the molecular dynamics program GROMACS, version 3.2.1 with a cutoff of 0.9 and 1.0 nm for XPLOR-NIH and ROSETTA structures, respectively (31). Atom density maps (see Fig. 3) were calculated by using VMD-XPLOR (32) and represent a 5% amplitude isosurface of the density of atoms in the peptide main chain of the structures comprising each cluster. Average contact maps were generated by using MOLMOL (33) (see Fig. 4 and Fig. 6, which is published as supporting information on the PNAS web site, for structures calculated by using XPLOR-NIH and ROSETTA, respectively).

Results and Discussion

Long-Range Interactions in the Native State of αS. The interaction between a specifically attached paramagnetic nitroxide radical and nearby (less than ≈25 Å) protons causes broadening of their NMR signals because of an increase in transverse relaxation rate (26). This effect has an r^{-6} dependence on the electron–proton distance and thus allows the detection of long-range interactions in proteins. The peak intensity ratios between the two ^{15}N-^{1}H HSQC NMR spectra, i.e., in the presence and absence of the nitroxide radical (I_{param}/I_{diam}), permit the estimation of distances between the spin label and the affected amide protons in the protein (14, 34).

Because the primary sequence of αS lacks cysteine, three different cysteine-containing mutants (A18C, A90C and A140C) were constructed to provide attachment points for the nitroxide radical MTSL. Neither the mere introduction of these mutations nor the addition of the MTSL radical modified the hydrodynamic radii or altered the time course of aggregation for αS (data not shown).

The effects of the nitroxide radical on the NMR spectra were very different for the three cysteine positions. (*i*) The profile of intensity ratios for the A18C mutant showed a broad paramagnetic effect extending to residue 60 and long-range interactions with C-terminal residues 115–140 (Fig. 1*a*). (*ii*) The paramagnetic tag at residue 90 strongly reduced the intensity ratios for all C-terminal residues (Fig. 1*b*). (*iii*) The A140C mutant showed an unbroadened core in the C terminus (residues 110–125), but a considerable PRE effect was present in the central region of the protein (residues 80–100) (Fig. 1*c*). Addition of 8 M urea led to a restriction of paramagnetic broadening to 15 residues from the position of the nitroxide radical (Fig. 1 *d* and *e*), indicating that the protein was fully unfolded. Interestingly, in the case of the A18C a considerable paramagnetic effect on the C terminus remained even under strong denaturant conditions. The extended relaxation enhancement observed in urea for the A140C (Fig. 1*f*) was likely caused by the very high flexibility of the C-terminal residue (34).

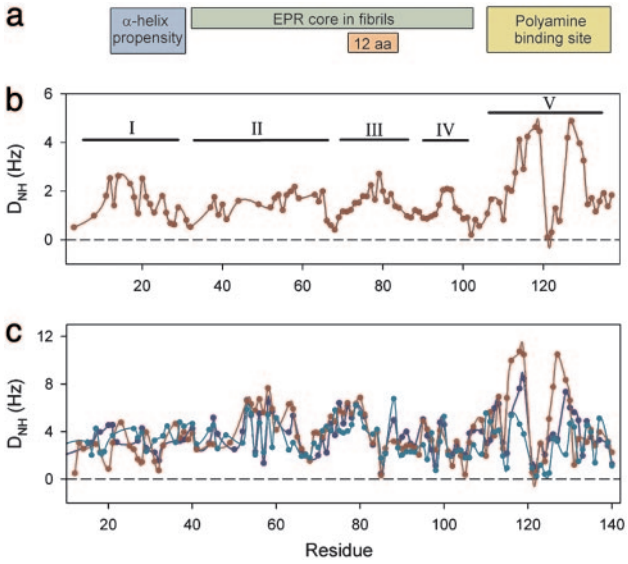

Fig. 2. RDCs in αS. N-H dipolar couplings at 15°C. (*a*) Functional domains of αS (7, 11, 19, 44). (*b*) RDC profile of αS aligned with Pf1 (red). (*c*) RDC profile of αS aligned with C8E5 in buffer A (red), plus 4 M urea (blue), or 8 M urea (cyan).

RDCs Detect a Hydrophobic Cluster in αS. The measurement of RDCs in a weakly aligned protein, for which the large one-bond internuclear dipolar interactions no longer average to zero, provides long-range orientational information (35). One-bond N-H RDCs ($^{1}D_{NH}$) were measured for αS aligned in bacteriophage Pf1 suspensions (20) and *n*-octyl-penta(ethylene glycol)/octanol (C8E5) (21) (Fig. 2). The highly reproducible RDC pattern in the two media and the absence of induced chemical shifts changes indicated that the alignment media did not appreciably perturb the ensemble of conformations (Fig. 7, which is published as supporting information on the PNAS web site).

In contrast to the bell-like smooth distribution of dipolar couplings that is expected for a random coil polypeptide chain (36), a very specific distribution of positive couplings was observed for αS (Fig. 2*a*). Five different domains can be identified. The N terminus is subdivided into two regions with similar RDCs (domain I: residues 1–28; domain II: residues 33–65) with a linker sequence showing couplings close to zero (residues 28–32). The NAC (non-Aβ component of Alzheimer's disease amyloid) domain (residues 61–95) exhibits large couplings about its central core, is flanked by two regions with reduced RDCs (residues 66–70 and 88–92), and is followed by a fourth domain (IV) comprising residues 95–105. The C terminus (domain V) displays exceptionally large couplings with two major peaks for residues 115–119 and 125–129.

The five domains identified by RDCs are consistent with the interpretations of previous biophysical studies (Fig. 2*a*). A weak α-helical propensity has been determined for the first domain (11), whereas RDC domain III overlays with the center of the NAC region. Domains II, III, and IV represent the part of αS that is highly ordered in fibrils (19), and domain V comprises the polyamine binding site (7). Linker regions with couplings close to zero can be rationalized by the presence of residues with predominantly small side chains (Ala^{29}-Ala^{30}-Gly^{31}, Gly^{67}-Gly^{68}-Ala^{69}, and Ala^{89}-Ala^{90}-Ala^{91}). Local interactions between side chains and the backbone are minimized, enabling higher flexi-

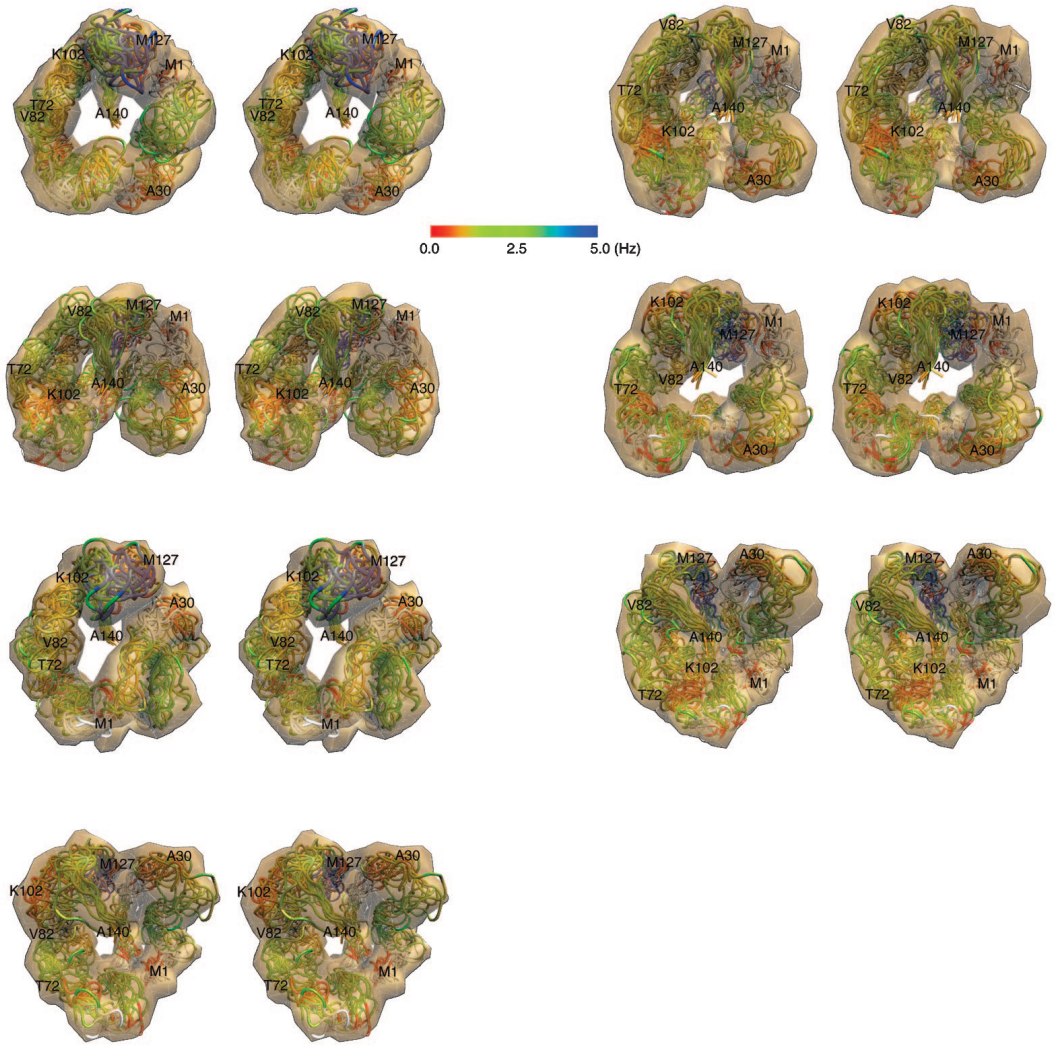

Fig. 3. Native-state conformations of αS. Representation of the native state of αS calculated from PRE data. Shown are the seven most populated clusters containing 80, 75, 46, 39, 25, 24, and 20 structures representing 50% of all calculated conformations. The 10 lowest-energy structures of each cluster within an atomic density map (32) calculated from all conformations contained in each cluster are shown. RDCs were mapped onto the structures with the use of a continuous color scale.

bility of the polypeptide backbone and effectively decoupling the five domains exhibiting concerted motion. The 100 N-terminal residues of αS assume a α-helical conformation upon binding to phospholipid membranes with helix fraying for residues 30–42, 60–65, and 82–100 (37). These regions of helix fraying roughly correlate with the hinge regions between RDC domains I and II, II and III, and the small RDC domain IV, indicating that the manner in which αS interacts with membranes is already encoded in its solution state.

The highly acidic C terminus of αS exhibited very large dipolar couplings. Addition of 4 and 8 M urea progressively decreased the RDC values in this region, down to a magnitude similar to the rest of the protein, whereas other features remained stable (Fig. 2*b*). Because urea mainly abolishes hydrophobic interactions, the RDCs are suggestive of a hydrophobic cluster in the C terminus involving residues 115–119 (Met^{116}, Val^{118}) and 125–129 (Tyr^{125}, Met^{127}). Additional information about this hydrophobic cluster was derived from RDCs measured for a C-terminal peptide of αS (residues 105–136). Although the overall RDC patterns for the peptide and the full-length protein were similar (Fig. 7*C*), the two regions showing very large RDCs in the case of the full-length protein were reduced, particularly for residues 125–129, suggesting that long-range interactions with other domains of the protein serve to stabilize this intrinsic structure. The 30% smaller RDC values for residues 75–81 in 8 M urea (Fig. 2*c*) and the strong paramagnetic broadening of the C terminus for the A90C mutant identify the hydrophobic NAC region as a major contributor.

Transverse relaxation rates have been used previously to probe long-range interactions within a nonnative protein (15). ^{15}N relaxation time measurements of αS did not provide evidence for long-range interactions, and only a very slight increase in R_2 relaxation rates for residues 20 and 122 was observed (11). Thus, the intrinsic structure present in αS restricts motions slower than the overall correlation time of the protein but faster than the millisecond motions probed by R_2 measurements. This range corresponds to the time scale for secondary structure formation in proteins (38).

The C Terminus of αS Shields the Central NAC Region. To determine an ensemble of conformations consistent with the PRE measurements, intensity ratios were converted into distance re-

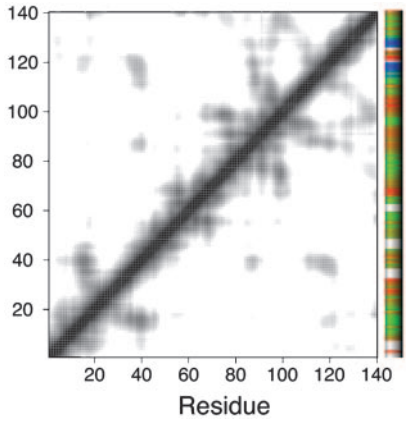

Fig. 4. Long-range interactions in αS. Average contact map for the center structures of the seven most populated clusters representing 50% of all calculated conformations. A continuous gray scale from 3 Å (black) to 22 Å (white) is used. RDCs as a function of residue number are indicated by a color bar.

straints. Inasmuch as large errors are associated with distances calculated from PRE data and intensity ratios are averages over a broad ensemble of structures, the calculated distances were used as semiquantitative restraints in structure calculations with XPLOR-NIH (26, 27). The seven most representative conformations of the native state of αS are shown in Fig. 3. The calculated structures represent temporal and distance averages over an ensemble of conformations, and thus may combine structural features that may not necessarily coexist in a given molecule. In particular, calculated structures are overly compact because of the r^{-6} distance dependence of paramagnetic broadening. The influence of the chosen computational strategy was tested by additional structure calculations with ROSETTA, in which hydrophobic burial and strand pairing as well as satisfaction of PRE restraints were favored (28, 29).

Favorable long-range interactions were extracted by an average contact map calculated from the center structures of these seven clusters representing 50% of 630 calculated structures (Fig. 4). The most important interaction is a hydrophobic cluster that comprises the C-terminal part of the highly hydrophobic NAC region (residues 85–95) and the C terminus (residues 110–130), probably mediated by Met^{116}, Val^{118}, Tyr^{125}, and Met^{127}. Within the C-terminal domain residues 120–130 contact residues 105–115, and the region about residue 120 also interacts with the N terminus about residue 20. These interactions presumably inhibit spontaneous αS oligomerization and are compatible with the influence in fibrillation exerted by methionine oxidation, tyrosine nitration, and phosphorylation of Ser^{129} (39, 40). Furthermore, shielding of the hydrophobic NAC region explains why the C-terminal acidic tail functions as a solubilizing domain for αS (41) and truncated αS is more amyloidogenic than the full-length protein (42). The compact state of native αS also involves a turn in the N terminus of the molecule (residues 20–30). This turn favors an ensemble of structures in which domain I, identified by RDCs (Fig. 2*a*), folds back onto domain II, a conformation that could be stabilized by the partial α-helical character of domain I (11). Dipolar couplings provide further support for key features visible in the calculated structures. Turn regions are associated mainly with small RDCs indicative of increased flexibility (e.g., residues 26–32), whereas more extended parts correspond to regions with large dipolar couplings (e.g., residues 72–82). The largest RDCs are located in the most compact structural region (residues 110–130) (Fig. 3).

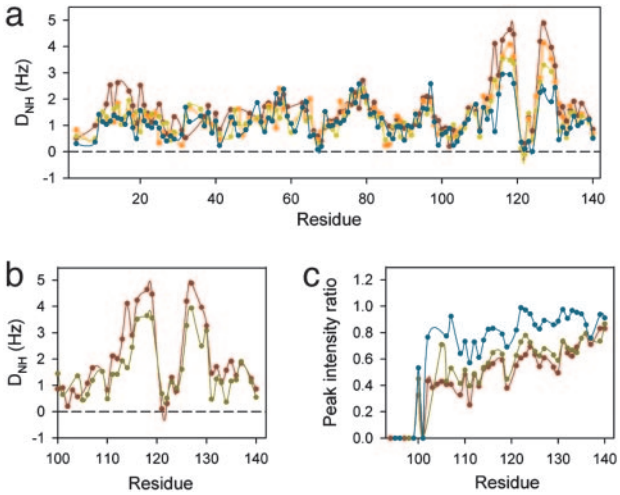

Fig. 5. Influence of aggregation prone conditions on long-range structure in αS. (*a*) Influence of polyamines on dipolar couplings. $^1D_{NH}$ couplings were measured at 15°C, for αS aligned in Pf1 phage (red) and in the presence of 3 mM putrescine (+2) (orange), 3 mM spermidine (+3) (green), and 3 mM spermine (+4) (cyan). (*b*) Influence of temperature on RDCs. C-terminal RDC profile of αS aligned with Pf1 at 15°C (red) and at 37°C (green). (*c*) Influence of temperature on PRE effects for the C terminus of αS A90C labeled with MTSL at 15°C (red), 37°C (green), and 47°C (cyan).

Polyamine Binding Releases Long-Range Interactions. To address the functional relevance of these long-range, intramolecular interactions, we performed the same experiments for conditions favoring aggregation, namely polycation binding and increased temperature. The polycation spermine is a naturally occurring polyamine that increases the kinetic efficiency of αS aggregation by 10^5 because of a specific interaction with the C terminus of the protein (7).

Upon addition of spermine, the PRE effects of residues 18–60 (A18C mutant) were considerably reduced (Fig. 1*g*), demonstrating that binding of polyamines to the C-terminal domain causes a release of the N terminus and thus an opening of the αS structure. This phenomenon is also consistent with the intensity increases of NMR signals of residues 22–93 resulting from polyamine binding (7). For the A90C mutant, binding of spermine led to a minimization of paramagnetic broadening in the C terminus, achieving a profile similar to that of the denaturated state in 8 M urea (Fig. 1 *e* and *h*). According to the A140C data, the presence of spermine also reduced the compactness of the region between residues 110 and 125 (Fig. 1*i*). Broadening in other regions of the protein reflects the increased flexibility of the C terminus and residual N-terminus/C-terminus interaction.

The large RDCs observed for the C terminus were reduced in the presence of polyamines (Figs. 5*a* and 7). Greater polyamine charge, putrescine (+2) < spermidine (+3) < spermine (+4), correlated with a stronger reduction in $^1D_{NH}$ values, as well as with an enhancement of fibrillation (7). In addition, binding of spermine to the C terminus reduced RDCs for residues 12–26 by ≈60%, indicating a long-range effect with the N terminus, in agreement with intensity increases of NMR signals of residues 22–93 upon polyamine binding (7). Such a decrease was not observed upon addition of urea, pointing to an electrostatic interaction between the negatively charged C terminus and the positively charged N terminus. The remaining paramagnetic broadening in the C terminus for the A18C mutant (Fig. 1*d*) indicates that the N-terminus/C-terminus interaction is not abolished upon addition of polyamines but only weakened, and that RDCs and PREs possess different sensitivities to the strength of long-range interactions.

Our data demonstrate that long-range interactions between the C terminus and the NAC region, presumably of hydrophobic nature, as well as the N terminus acting via electrostatic interactions, protect αS from oligomerization. Docking of polycations to the C terminus destabilizes these interactions. The high free energy of the extended conformation, in which the hydrophobic NAC region is exposed to the solvent, would favor the association of monomers, thereby increasing the extent of both the nucleation and propagation steps of aggregation (7).

The Residual Structure of Native αS Is Lost at Elevated Temperatures. The rate of fibrillation increases when αS is incubated at increasing temperatures (6). Comparison of RDCs measured at 15°C and 37°C showed a decrease in the coupling values for both subdomains of the C terminus at the higher temperature (Fig. 5*b*). This result correlated well with further evidence obtained from PRE studies on the A90C mutant. At 37°C the paramagnetic effect on the C terminus was similar to the one at 15°C, whereas at 47°C, virtually no paramagnetic broadening remained for resonances beyond residue 105 (Fig. 5*c*). We conclude that at elevated temperatures the C terminus of αS adopts a fully extended conformation, similar to the one achieved upon addition of denaturant or polycation. It is noteworthy that the changes in RDCs are already evident, but the PRE broadening remains unchanged. This result is in agreement with the proposal that destabilization of long-range interactions initially releases the stiffness of the polypeptide chain (as probed by the decrease in RDCs) followed by an opening of the tertiary structure (as monitored by PRE effects). We conclude that RDCs provide a very powerful tool for probing structural transitions in unfolded proteins.

Stabilization of Autoinhibitory Interactions in αS May Inhibit Aggregation in PD. This study demonstrates that native αS populates an ensemble of conformations comprising a continuum of conformers ranging from highly unfolded to fairly compact. Although highly dynamic, the ensemble of conformers is stabilized by long-range, i.e., tertiary, interactions, leading to compaction of both the N and C termini coupled to a flip-back of the C terminus over the central region of the protein. Such a model explains why the hydrodynamic radius of αS corresponds to that of a completely unfolded polypeptide chain in the presence of 8 M urea, but is considerably smaller in the native state (43). *In vivo*, the native compaction is likely to be further stabilized by the strong excluded volume effects associated with macromolecular crowding. We conclude that the release of intrinsic structure in the αS monomer is a or the key step that triggers oligomerization and aggregation. That is, the achievement of the fully unfolded state renders the hydrophobic patches of the NAC region accessible, and the N terminus fully extended, such that the protein is able to adopt β-sheet conformations conducive to aggregation. It follows that alterations in the energetic barriers to achieve this conformational transition would affect the deposition rate of αS aggregates *in vivo* and thus the evolution of disease. From the therapeutic point of view, the reinforcement of these native, autoinhibitory, long-range interactions in αS constitutes a logical functional target for new pharmacological agents designed to impede or even reverse aggregate formation in PD.

We thank K. Overkamp for synthesis of the C-terminal αS peptide. This work was supported by the Max-Planck-Gesellschaft (T.M.J. and C.G.), Deutsche Forschungsgemeinschaft Emmy Noether Fellowship ZW 71/1-4 (to M.Z.), Deutsche Forschungsgemeinschaft Grant GK 782 (to C.G.), and the Fonds der Chemischen Industrie. C.O.F. received a fellowship from the A. V. H. Foundation and thanks Fundacion Antorchas and the Agencia Nacional de Promoción Cientifica y Tecnológica for financial support. This work was within the scientific scope of the Deutsche Forschungsgemeinschaft Center for Molecular Physiology of the Brain in Göttingen (C.G., T.M.J., and M.Z.).

1. Goedert, M. (2001) *Nat. Rev. Neurosci.* **2,** 492–501.
2. Dawson, T. M. & Dawson, V. L. (2003) *Science* **302,** 819–822.
3. Spillantini, M. G., Schmidt, M. L., Lee, V. M., Trojanowski, J. Q., Jakes, R. & Goedert, M. (1997) *Nature* **388,** 839–840.
4. Dawson, T. M. & Dawson, V. L. (2003) *J. Clin. Invest.* **111,** 145–151.
5. Zarranz, J. J., Alegre, J., Gomez-Esteban, J. C., Lezcano, E., Ros, R., Ampuero, I., Vidal, L., Hoenicka, J., Rodriguez, O., Atares, B., *et al*. (2004) *Ann. Neurol.* **55,** 164–173.
6. Uversky, V. N., Li, J. & Fink, A. L. (2001) *J. Biol. Chem.* **276,** 10737–10744.
7. Fernandez, C. O., Hoyer, W., Zweckstetter, M., Jares-Erijman, E. A., Subramaniam, V., Griesinger, C. & Jovin, T. M. (2004) *EMBO J.* **23,** 2039–2046.
8. Lansbury, P. T., Jr. & Brice, A. (2002) *Curr. Opin. Cell. Biol.* **14,** 653–660.
9. Dobson, C. M. (2003) *Nature* **426,** 884–890.
10. Weinreb, P. H., Zhen, W., Poon, A. W., Conway, K. A. & Lansbury, P. T., Jr. (1996) *Biochemistry* **35,** 13709–13715.
11. Bussell, R., Jr. & Eliezer, D. (2001) *J. Biol. Chem.* **276,** 45996–46003.
12. Hoyer, W., Cherny, D., Subramaniam, V. & Jovin, T. M. (2004) *Biochemistry* **43,** 16233–16242.
13. Dyson, H. J. & Wright, P. E. (1998) *Nat. Struct. Biol.* **5,** Suppl., 499–503.
14. Lietzow, M. A., Jamin, M., Dyson, H. J. & Wright, P. E. (2002) *J. Mol. Biol.* **322,** 655–662.
15. Klein-Seetharaman, J., Oikawa, M., Grimshaw, S. B., Wirmer, J., Duchardt, E., Ueda, T., Imoto, T., Smith, L. J., Dobson, C. M. & Schwalbe, H. (2002) *Science* **295,** 1719–1722.
16. Shortle, D. & Ackerman, M. S. (2001) *Science* **293,** 487–489.
17. Mohana-Borges, R., Goto, N. K., Kroon, G. J., Dyson, H. J. & Wright, P. E. (2004) *J. Mol. Biol.* **340,** 1131–1142.
18. Hoyer, W., Antony, T., Cherny, D., Heim, G., Jovin, T. M. & Subramaniam, V. (2002) *J. Mol. Biol.* **322,** 383–393.
19. Der-Sarkissian, A., Jao, C. C., Chen, J. & Langen, R. (2003) *J. Biol. Chem.* **278,** 37530–37535.
20. Hansen, M. R., Mueller, L. & Pardi, A. (1998) *Nat. Struct. Biol.* **5,** 1065–1074.
21. Rückert, M. & Otting, G. (2000) *J. Am. Chem. Soc.* **122,** 7793–7797.
22. Ottiger, M., Delaglio, F. & Bax, A. (1998) *J. Magn. Res.* **131,** 373–378.
23. Bax, A. & Grzesiek, S. (1993) *Acc. Chem. Res.* **26,** 131–138.
24. Delaglio, F., Grzesiek, S., Vuister, G. W., Zhu, G., Pfeifer, J. & Bax, A. (1995) *J. Biomol. NMR* **6,** 277–293.
25. Johnson, B. A. & Blevins, R. A. (1994) *J. Biomol. NMR* **4,** 603–614.
26. Gillespie, J. R. & Shortle, D. (1997) *J. Mol. Biol.* **268,** 158–169.
27. Schwieters, C. D., Kuszewski, J. J., Tjandra, N. & Clore, G. M. (2003) *J. Magn. Reson.* **160,** 65–73.
28. Simons, K. T., Kooperberg, C., Huang, E. & Baker, D. (1997) *J. Mol. Biol.* **268,** 209–225.
29. Bowers, P. M., Strauss, C. E. & Baker, D. (2000) *J. Biomol. NMR* **18,** 311–318.
30. Bolin, K. A., Pitkeathly, M., Miranker, A., Smith, L. J. & Dobson, C. M. (1996) *J. Mol. Biol.* **261,** 443–453.
31. Lindahl, E., Hess, B. & van der Spoel, D. (2001) *J. Mol. Model.* **7,** 306–317.
32. Schwieters, C. D. & Clore, G. M. (2002) *J. Biomol. NMR* **23,** 221–225.
33. Koradi, R., Billeter, M. & Wuthrich, K. (1996) *J. Mol. Graphics* **14,** 51–55.
34. Teilum, K., Kragelund, B. B. & Poulsen, F. M. (2002) *J. Mol. Biol.* **324,** 349–357.
35. Tjandra, N. & Bax, A. (1997) *Science* **278,** 1111–1114.
36. Louhivuori, M., Pääkkönen, K., Fredriksson, K., Permi, P., Lounila, J. & Annila, A. (2003) *J. Am. Chem. Soc.* **125,** 15647–15650.
37. Chandra, S., Chen, X. C., Rizo, J., Jahn, R. & Sudhof, T. C. (2003) *J. Biol. Chem.* **278,** 15313–15318.
38. Kubelka, J., Hofrichter, J. & Eaton, W. A. (2004) *Curr. Opin. Struct. Biol.* **14,** 76–88.
39. Norris, E. H., Giasson, B. I., Ischiropoulos, H. & Lee, V. M. Y. (2003) *J. Biol. Chem.* **278,** 27230–27240.
40. Fujiwara, H., Hasegawa, M., Dohmae, N., Kawashima, A., Masliah, E., Goldberg, M. S., Shen, J., Takio, K. & Iwatsubo, T. (2002) *Nat. Cell. Biol.* **4,** 160–164.
41. Souza, J. M., Giasson, B. I., Lee, V. M. & Ischiropoulos, H. (2000) *FEBS Lett.* **474,** 116–119.
42. Crowther, R. A., Jakes, R., Spillantini, M. G. & Goedert, M. (1998) *FEBS Lett.* **436,** 309–312.
43. Uversky, V. N., Li, J., Souillac, P., Millett, I. S., Doniach, S., Jakes, R., Goedert, M. & Fink, A. L. (2002) *J. Biol. Chem.* **277,** 11970–11978.
44. Giasson, B. I., Murray, I. V., Trojanowski, J. Q. & Lee, V. M. (2001) *J. Biol. Chem.* **276,** 2380–2386.